 CMES, vol.13, no.2, pp.103-117, 2006

Meshless Local Petrov-Galerkin (MLPG) Method for Shear Deformable Shells Analysis

J. Sladek[1], V. Sladek[1], P. H. Wen[2], M.H. Aliabadi[3]

Abstract: A meshless local Petrov-Galerkin (MLPG) method is applied to solve bending problems of shear deformable shallow shells described by the Reissner theory. Both static and dynamic loads are considered. For transient elastodynamic case the Laplace-transform is used to eliminate the time dependence of the field variables. A weak formulation with a unit test function transforms the set of governing equations into local integral equations on local subdomains in the mean surface of the shell. Nodal points are randomly spread on that surface and each node is surrounded by a circular subdomain to which local integral equations are applied. The meshless approximation based on the Moving Least-Squares (MLS) method is employed for the implementation. Unknown Laplace-transformed quantities are computed from the local boundary integral equations. The time-dependent values are obtained by the Stehfest's inversion technique.

keyword: Reissner theory, local boundary integral equations, Laplace-transform, Stehfest's inversion, MLS approximation, static and impact loads

1 Introduction

In recent years the demand for construction of huge and lightweight shell and spatial structures has been increasing. Generally, numerical methods are required to solve such analysis with complex loading and geometry, as analytical solution is not possible. For the last three decades, some numerical methods such as Finite Difference Method (FDM) and Finite Element Method (FEM) have been successfully developed to solve the problems. Boundary Element Method (BEM) has been emerged as an alternative numerical method to solve plate and shell problems. A review article devoted to early applications of BEM to shells is given by Beskos (1991). The first application of BEM to shells is given by Newton and Tottenham (1968, 1979), where they presented a method based on the decomposition of the fourth-order governing equation into a set of the second-order ones. Antes (1981) derived a BEM formulation for circular spherical shells. Tosaka and Miyake (1983) developed a direct BEM formulation for shallow shells. Lu and Huang (1992) derived a direct BEM formulation for shallow shells involving shear deformation. Wang and Schweizerhof (1996a) applied boundary integral equation method for moderately thick laminated orthotropic shallow shells. For elastodynamic shell problems it is appropriate to use the weighted residual method with static fundamental solution as a test function [Zhang and Atluri (1986), Wang and Schweizerhof (1996b,c); Providakis and Beskos (1991)]. Dirgantara and Aliabadi (1999) applied the domain-boundary element method for shear deformable shells under a static load. They used a test function corresponding to thick plate bending problem. Ling and Long (1996) used this method for geometrically nonlinear analysis of shallow shells.

In spite of the great success of the FEM and the BEM as accurate and effective numerical tools for the solution of boundary value problems with complex domains, there is still a growing interest in developing new advanced numerical methods. In recent years, meshfree or meshless formulations are becoming to be popular due to their high adaptivity and low costs to prepare input data for numerical analyses. A variety of meshless methods has been proposed so far [Belytschko et al. (1994); Atluri and Shen (2002); Atluri (2004)]. Many of them are derived from a weak-form formulation on global domain [Belytschko et al. (1994)] or a set of local subdomains [Atluri et al. (2000, 2003); Han and Atluri (2004a,b), Mikhailov (2002); Sellountos and Polyzos (2003); Sellountos et al. (2005)]. In the global formulation background cells are required for the integration of the weak-

[1] Institute of Construction and Architecture, Slovak Academy of Sciences, 84503 Bratislava, Slovakia

[2] Department of Engineering, Queen Mary University of London, Mile End, London E14 NS, U.K.

[3] Department of Aeronautics, Imperial College London, Prince Consort Road, London SW7 2BY, U.K.

form. In methods based on local weak-form formulation no cells are required and therefore they are often referred to as truly meshless methods. If a simple form is chosen for the geometry of the subdomains, numerical integrations can be easily carried out over them. The meshless local Petrov-Galerkin (MLPG) method is a fundamental base for the derivation of many meshless formulations, since trial and test functions can be chosen from different functional spaces. The method has been successfully applied also to plate problems [Sladek et al. (2002, 2003); Long and Atluri (2002); Soric et al. (2004)].

The first application of meshless method to for plate/shell problems was given by Krysl and Belytschko (1985, 1996), where they applied element-free Galerkin method. The moving least-square approximation yields C^1 continuity which satisfies the Kirchhoff hypothesis. Their results showed excellent convergence, however, their formulation is not applicable to shear deformable plate/shell problems. Recently, Noguchi et al. (2000) used a mapping technique to transform the curved surface into flat two-dimensional space. Then, the element-free Galerkin method can be applied also to thick plates or shells including the shear deformation effects.

In the present paper, we have developed for the first time a meshless method based on the local Petrov-Galerkin weak-form to solve dynamic shell problems described by the Reissner theory. Nodal points are randomly distributed over the mean surface of the considered shell. Each node is the center of a circle surrounding this node. Similar approach has been successfully applied to a thin Kirchhoff plate [Sladek et al (2002, 2003)] and recently also to thick plates [Sladek et al (2005)]. In this paper, the Laplace-transform technique is applied to the set of governing differential equations for elastodynamic Reissner shell bending theory. A unit test function is used in the local weak-form of the governing equations for transformed fields. Applying the Gauss divergence theorem to the weak-form, the local boundary-domain integral equations are derived. The numerical integration of the domain integrals arising from the inertial term and the initial values on a simple domain does not give rise to difficulties if the meshless approximation based on the Moving Least-Squares (MLS) method is utilized. The quasi-static boundary value problems must be solved for several values of the Laplace-transform parameter selected for each considered time instant. The Stehfest's inversion method [Stehfest (1970)] is employed to obtain the time-dependent solution.

Numerical results for circular and square shallow spherical shells with different boundary conditions and subjected to static and impulsive loads are presented to illustrate the accuracy and efficiency of the proposed method. Comparisons of the present numerical results with the FEM results show good agreement.

2 Local integral equations for shear deformable shells

Consider an elastic shallow shell of the constant thickness h and with its mid surface being described by $x_3 = f(x_1,x_2)$in a domain Ω with the boundary contour Γ in the base plane $x_1 - x_2$. The shell is subjected to a transient dynamic load $q_i(\mathbf{x},t)$. Using the Reissner's linear theory of shallow shells [Reissner (1946)], the equilibrium equations may be written as

$$M_{\alpha\beta,\beta}(\mathbf{x},t) - Q_\alpha(\mathbf{x},t) = \frac{\rho h^3}{12}\ddot{w}_\alpha(\mathbf{x},t) \quad ,$$

$$Q_{\alpha,\alpha}(\mathbf{x},t) - k_{\alpha\beta}N_{\alpha\beta}(\mathbf{x},t) + q_3(\mathbf{x},t) = \rho h\ddot{w}_3(\mathbf{x},t)$$

$$N_{\alpha\beta,\beta}(\mathbf{x},t) + q_\alpha(\mathbf{x},t) = \rho\ddot{u}_\alpha(\mathbf{x},t) \quad \mathbf{x}\in\Omega \quad , \tag{1}$$

where ρ is the mass density, w_3 represent the out-of-plane deflection, while u_α and w_α denote the in-plane displacements and the rotation in the x_α-direction, respectively, $M_{\alpha\beta}$ represent the bending moments, $N_{\alpha\beta}$ are normal stress resultants, q_i are body forces, and Q_α are the shear forces. Latin indices vary from 1 to 3 and Greek indices vary from 1 to 2. The dots indicate differentiations with respect to time t. The principal curvatures of the shell in x_1 and x_2 are denoted by k_{11} and k_{22}, respectively and $k_{12} = k_{21} = 0$.

The bending moments $M_{\alpha\beta}$, normal force stress $N_{\alpha\beta}$, and the shear forces Q_α are expressed in terms of the rotations, the lateral displacement and in-plane displacements u_α as

$$M_{\alpha\beta} = \frac{1-\nu}{2}D\left(w_{\alpha,\beta} + w_{\beta,\alpha} + \frac{2\nu}{1-\nu}w_{\gamma,\gamma}\delta_{\alpha\beta}\right) \quad ,$$

$$Q_\alpha = \frac{D(1-\nu)}{2}\lambda^2\left(w_\alpha + w_{3,\alpha}\right) \quad ,$$

$$N_{\alpha\beta} = \frac{1-\nu}{2} B \left(u_{\alpha,\beta} + u_{\beta,\alpha} + \frac{2\nu}{1-\nu} u_{\gamma,\gamma} \delta_{\alpha\beta} \right) + B \left[(1-\nu) k_{\alpha\beta} + \nu \delta_{\alpha\beta} k_{\gamma\gamma} \right] w_3 \quad , \tag{2}$$

where $D = Eh^3/12(1-\nu^2)$ denotes the bending stiffness of the shell, with E being Young's modulus, ν being Poisson's ratio, and $\lambda^2 = 10/h^2$ is the shear correction factor of the Reissner theory, $B = Eh/(1-\nu^2)$ is the tension stiffness.

To eliminate the time variable t in the equilibrium equations (1), the Laplace-transform

$$L[f(\mathbf{x},t)] = \overline{f}(\mathbf{x},s) = \int_0^\infty f(\mathbf{x},t) e^{-st} dt \tag{3}$$

is applied to this system of governing equations. Then, one can write

$$\overline{M}_{\alpha\beta,\beta}(\mathbf{x},s) - \overline{Q}_\alpha(\mathbf{x},s) = \frac{\rho h^3}{12} s^2 \overline{w}_\alpha(\mathbf{x},s) - \overline{R}_\alpha(\mathbf{x},s) \tag{4}$$

$$\overline{Q}_{\alpha,\alpha}(\mathbf{x},s) - k_{\alpha\beta} \overline{N}_{\alpha\beta}(\mathbf{x},s) = \rho h s^2 \overline{w}_3(\mathbf{x},s) - \overline{R}_3(\mathbf{x},s), \tag{5}$$

$$\overline{N}_{\alpha\beta,\beta}(\mathbf{x},s) = \rho s^2 \overline{u}_\alpha(\mathbf{x},s) - \overline{R'}_\alpha(\mathbf{x},s) \quad , \tag{6}$$

where s is the Laplace-transform parameter, $\overline{R}_\alpha$,$\overline{R}_3$ and $\overline{R}'_\alpha$ are given by

$$\overline{R}_\alpha(\mathbf{x},s) = \frac{\rho h^3}{12} \left[s w_\alpha(\mathbf{x}) + \dot{w}_\alpha(\mathbf{x}) \right],$$

$$\overline{R}_3(\mathbf{x},s) = \overline{q}_3(\mathbf{x},s) + \rho h s w_3(\mathbf{x}) + \rho h \dot{w}_3(\mathbf{x}),$$

$$\overline{R}'_\alpha(\mathbf{x},s) = \overline{q}_\alpha(\mathbf{x},s) + \rho s u_\alpha(\mathbf{x}) + \rho \dot{u}_\alpha(\mathbf{x}),$$

with $w_k(\mathbf{x})$, $u_\alpha(\mathbf{x})$ and $\dot{w}_k(\mathbf{x})$, $\dot{u}_\alpha(\mathbf{x})$ being the initial values and the initial velocities of the considered quantities.

A rather simple case can be presented by steady-state harmonic oscillations, when the time-dependence of all the physical quantities is known *a priori*, since

$$A(\mathbf{x},t) = A^*(\mathbf{x},\omega) e^{-i\omega t},$$

where $A^*(\mathbf{x},\omega)$ is the amplitude of the corresponding physical quantities and ω is the circular frequency of the oscillations. Then, the governing equations (4) - (6) become

$$M^*_{\alpha\beta,\beta}(\mathbf{x},\omega) - Q^*_\alpha(\mathbf{x},\omega) = -\frac{\rho h^3}{12} \omega^2 w^*_\alpha(\mathbf{x},\omega) \quad ,$$

$$Q^*_{\alpha,\alpha}(\mathbf{x},\omega) - k_{\alpha\beta} N^*_{\alpha\beta}(\mathbf{x},\omega) + q^*_3(\mathbf{x},\omega) = -\rho h \omega^2 w^*_3(\mathbf{x},\omega) \quad ,$$

$$N^*_{\alpha\beta,\beta}(\mathbf{x},\omega) + q^*_\alpha(\mathbf{x},\omega) = -\rho \omega^2 u^*_\alpha(\mathbf{x},\omega). \tag{7}$$

Comparing eqs. (7) with eqs. (4), (5) and (6), it is seen that they are formally the same for $s = -i\omega$ and for vanishing initial conditions. Therefore, the harmonic case is not analysed separately in this paper.

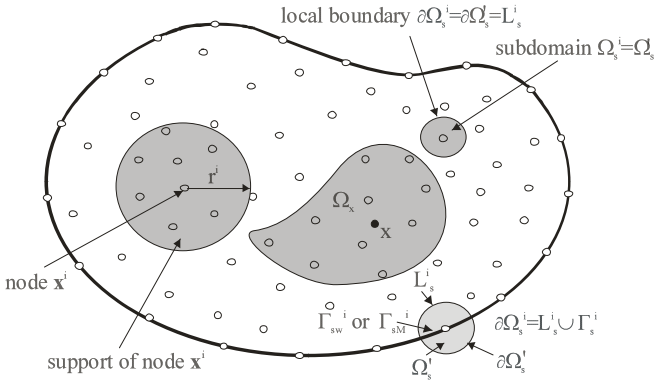

Figure 1 : Local boundaries for weak formulation, the domain Ω_x for MLS approximation of the trial function, and support area of weight function around node $\mathbf{x}^i$

Instead of writing the global weak-form for the above governing equations, the MLPG methods construct the weak-form over local subdomains such as Ω_s, which is a small region taken for each node inside the global domain [Atluri (2004)]. The local subdomains overlap each other and cover the whole global domain Ω (Fig. 1). The local subdomains could be of any geometrical shape and size. In the current paper, the local subdomains are taken to be of circular shape. The local weak-form of the governing equations (4), (5) and (6) for $\mathbf{x}^i \in \Omega^i_s$ can be written as

$$\int_{\Omega^i_s} \left[\overline{M}_{\alpha\beta,\beta}(\mathbf{x},s) - \overline{Q}_\alpha(\mathbf{x},s) - \frac{\rho h^3}{12} s^2 \overline{w}_\alpha(\mathbf{x},s) + \overline{R}_\alpha(\mathbf{x},s) \right] w^*_{\alpha\gamma}(\mathbf{x}) d\Omega = 0 \quad , \tag{8}$$

$$\int_{\Omega^i_s} \left[\overline{Q}_{\alpha,\alpha}(\mathbf{x},s) - k_{\alpha\beta} \overline{N}_{\alpha\beta}(\mathbf{x},s) - \rho h s^2 \overline{w}_3(\mathbf{x},s) + \overline{R}_3(\mathbf{x},s) \right] w^*(\mathbf{x}) d\Omega = 0 \, , \tag{9}$$

$$\int_{\Omega_s^i} \left[\overline{N}_{\alpha\beta,\beta}(\mathbf{x},s) - \rho s^2 \overline{u}_\alpha(\mathbf{x},s) + \overline{R'}\alpha(\mathbf{x},s)\right] u^*_{\alpha\gamma}(\mathbf{x}) d\Omega = 0, \tag{10}$$

where $w^*_{\alpha\beta}(\mathbf{x})$, $u^*_{\alpha\beta}(\mathbf{x})$ and $w^*(\mathbf{x})$ are weight (test) functions.

Applying the Gauss divergence theorem to eqs. (8) - (10) one obtains

$$\begin{aligned}
&\int_{\partial\Omega_s^i} \overline{M}_\alpha(\mathbf{x},s) w^*_{\alpha\gamma}(\mathbf{x}) d\Gamma \\
&\quad - \int_{\Omega_s^i} \left[\overline{M}_{\alpha\beta}(\mathbf{x},s) w^*_{\alpha\gamma,\beta}(\mathbf{x}) + \overline{Q}_\alpha(\mathbf{x},s) w^*_{\alpha\gamma}(\mathbf{x})\right] d\Omega \\
&\quad - \int_{\Omega_s^i} \left(\frac{\rho h^3}{12} s^2 \overline{w}_\alpha(\mathbf{x},s) - \overline{R}_\alpha(\mathbf{x},s)\right) w^*_{\alpha\gamma}(\mathbf{x}) d\Omega = 0, \quad (11)
\end{aligned}$$

$$\begin{aligned}
&\int_{\partial\Omega_s^i} \overline{Q}_\alpha(\mathbf{x},s) n_\alpha(\mathbf{x}) w^*(\mathbf{x}) d\Gamma \\
&\quad - \int_{\Omega_s^i} \left[\overline{Q}_\alpha(\mathbf{x},s) w^*_{,\alpha}(\mathbf{x}) + k_{\alpha\beta}(\mathbf{x}) \overline{N}_{\alpha\beta}(\mathbf{x},s) w^*(\mathbf{x})\right] d\Omega \\
&\quad - \int_{\Omega_s^i} \left(\rho h s^2 \overline{w}_3(\mathbf{x},s) - \overline{R}_3(\mathbf{x},s)\right) w^*(\mathbf{x}) d\Omega = 0 \quad , \quad (12)
\end{aligned}$$

$$\begin{aligned}
&\int_{\partial\Omega_s^i} \overline{P}_\alpha(\mathbf{x},s) u^*_{\alpha\gamma}(\mathbf{x}) d\Gamma \\
&\quad - \int_{\Omega_s^i} \Big[\overline{N}_{\alpha\beta}(\mathbf{x},s) u^*_{\alpha\gamma,\beta}(\mathbf{x}) \\
&\quad + \left(\rho s^2 \overline{u}_\alpha(\mathbf{x},s) - \overline{R}'_\alpha(\mathbf{x},s)\right) u^*_{\alpha\gamma}(\mathbf{x})\Big] d\Omega = 0, \quad (13)
\end{aligned}$$

where $\partial\Omega_s^i$ is the boundary of the local subdomain and

$$\overline{M}_\alpha(\mathbf{x},s) = \overline{M}_{\alpha\beta}(\mathbf{x},s) n_\beta(\mathbf{x}),$$

$$\overline{P}_\alpha(\mathbf{x},s) = \overline{N}_{\alpha\beta}(\mathbf{x},s) n_\beta(\mathbf{x})$$

are the Laplace-transforms of the normal bending moments and traction vector, and n_α is the outward unit normal vector to the boundary. The local weak-forms (11) - (13) are a starting point for derivation of local boundary-domain integral equations with choosing appropriate test functions. A unit step function can be used as the test functions $w^*_{\alpha\beta}(\mathbf{x})$, $u^*_{\alpha\beta}(\mathbf{x})$ and $w^*(\mathbf{x})$ in each subdomain

$$w^*_{\alpha\gamma}(\mathbf{x}) = u^*_{\alpha\gamma}(\mathbf{x}) = \begin{cases} \delta_{\alpha\gamma} \text{ at } \mathbf{x} \in (\Omega_s \cup \partial\Omega_s) \\ 0 \quad \text{at } \mathbf{x} \notin (\Omega_s \cup \partial\Omega_s) \end{cases},$$

$$u^*(\mathbf{x}) = \begin{cases} 1 \quad \text{at } \mathbf{x} \in (\Omega_s \cup \partial\Omega_s) \\ 0 \quad \text{at } \mathbf{x} \notin (\Omega_s \cup \partial\Omega_s) \end{cases}. \tag{14}$$

Then, the local weak-forms (11) - (13) are transformed into simple local boundary-domain integral equations

$$\begin{aligned}
&\int_{\partial\Omega_s^i} \overline{M}_\alpha(\mathbf{x},s) d\Gamma - \int_{\Omega_s^i} \overline{Q}_\alpha(\mathbf{x},s) d\Omega \\
&\quad - \int_{\Omega_s^i} \frac{\rho h^3}{12} s^2 \overline{w}_\alpha(\mathbf{x},s) d\Omega + \int_{\Omega_s^i} \overline{R}_\alpha(\mathbf{x},s) d\Omega = 0 \quad , \quad (15)
\end{aligned}$$

$$\begin{aligned}
&\int_{\partial\Omega_s^i} \overline{Q}_\alpha(\mathbf{x},s) n_\alpha(\mathbf{x}) d\Gamma - \int_{\Omega_s^i} k_{\alpha\beta}(\mathbf{x}) \overline{N}_{\alpha\beta}(\mathbf{x},s) d\Omega \\
&\quad - \int_{\Omega_s^i} \rho h s^2 \overline{w}_3(\mathbf{x},s) d\Omega + \int_{\Omega_s^i} \overline{R}_3(\mathbf{x},s) d\Omega = 0 \quad , \quad (16)
\end{aligned}$$

$$\int_{\partial\Omega_s^i} \overline{P}_\alpha(\mathbf{x},s) d\Gamma - \int_{\Omega_s^i} \rho s^2 \overline{u}_\alpha(\mathbf{x},s) d\Omega + \int_{\Omega_s^i} \overline{R}'_\alpha(\mathbf{x},s) d\Omega = 0. \tag{17}$$

In the MLPG method the test and the trial functions are not necessarily from the same functional spaces. The test function is chosen as the unit step function with support on the local subdomain. The trial function, on the other hand, is chosen to be the moving least-squares (MLS) interpolation over a number of nodes randomly spread within the domain of influence, as described in more details in the next paragraph.

3 Numerical solution

In general, a meshless method uses a local interpolation to represent the trial function with the values (or the fictitious values) of the unknown variable at some randomly

located nodes. The moving least-squares (MLS) approximation [Lancaster and Salkauskas (1981), Nayroles et al. (1992), Atluri (2004)] used in the present analysis may be considered as one of such schemes. Let us consider a sub-domain Ω_x of the problem domain Ω in the neighbourhood of a point $\mathbf{x}$ for the definition of the MLS approximation of the trial function around $\boldsymbol{x}$ (Fig. 1). To approximate the distribution of the Laplace-transform of the generalized displacements (rotations and deflection) in Ω_x over a number of randomly located nodes $\{\mathbf{x}^a\}$, $a = 1,2,...n$, the MLS approximant $\overline{w}_i^h(\mathbf{x},s)$ of $\overline{w}_i$ is defined by

$$\overline{\mathbf{w}}^h(\mathbf{x},s) = \mathbf{p}^T(\mathbf{x})\tilde{\mathbf{a}}(\mathbf{x},s)\,, \quad \forall \mathbf{x} \in \Omega_x \tag{18}$$

where $\overline{\mathbf{w}}^h = \left[\overline{w}_1^h, \overline{w}_2^h, \overline{w}_3^h\right]^T$, $\mathbf{p}^T(\mathbf{x}) = \left[p^1(\mathbf{x}), p^2(\mathbf{x}), ..., p^m(\mathbf{x})\right]$ is a complete monomial basis of the order m, and $\tilde{\mathbf{a}}(\mathbf{x},s) = \left[\mathbf{a}^1(\mathbf{x},s), \mathbf{a}^2(\mathbf{x},s), ..., \mathbf{a}^m(\mathbf{x},s)\right]^T$ is composed of vectors $\mathbf{a}^j(\mathbf{x},s) = \left[a_1^j(\mathbf{x},s), a_2^j(\mathbf{x},s), a_3^j(\mathbf{x},s)\right]^T$ which are functions of the space co-ordinates $\mathbf{x} = [x_1, x_2, x_3]^T$ and the transform- parameter s. For example, for a two-dimensional (2-d) problem

$$\mathbf{p}^T(\mathbf{x}) = [1,\, x_1,\, x_2]\,, \quad \text{for linear basis } m = 3 \tag{19a}$$

$$\mathbf{p}^T(\mathbf{x}) = \left[1,\, x_1,\, x_2,\, (x_1)^2,\, x_1x_2,\, (x_2)^2\right], \quad \text{for quadratic basis } m = 6 \tag{19b}$$

Usually quadratic monomials are sufficient and they have been applied also in the numerical computations presented in this paper.

The coefficient vector $\tilde{\mathbf{a}}(\mathbf{x},s)$ is determined by minimizing a weighted discrete L_2-norm defined as

$$J(\mathbf{x}) = \sum_{a=1}^{n} v^a(\mathbf{x}) \left[\mathbf{p}^T(\mathbf{x}^a)\tilde{\mathbf{a}}(\mathbf{x},s) - \hat{\mathbf{w}}^a(s)\right]^2, \tag{20}$$

where $v^a(\mathbf{x}) > 0$ is the weight function associated with the node a and the square power is considered in the sense of scalar product. Recall that n is the number of nodes in Ω_x for which the weight function $v^a(\mathbf{x}) > 0$ and $\hat{\mathbf{w}}^a(s)$ are the fictitious nodal values, but not the nodal values of the unknown trial function $\overline{\mathbf{w}}^h(\mathbf{x},s)$ in general. The stationarity of J in eq. (20) with respect to $\tilde{\mathbf{a}}(\mathbf{x},s)$

$$\partial J/\partial \tilde{\mathbf{a}} = 0$$

leads to the following linear relation between $\tilde{\mathbf{a}}(\mathbf{x},s)$ and $\hat{\mathbf{w}}(s)$

$$\mathbf{A}(\mathbf{x})\tilde{\mathbf{a}}(\mathbf{x},s) - \mathbf{B}(\mathbf{x})\hat{\mathbf{w}}(s) = 0, \tag{21}$$

where

$$\hat{\mathbf{w}}(s) = \left[\hat{\mathbf{w}}^1(s), \hat{\mathbf{w}}^2(s), ..., \hat{\mathbf{w}}^n(s)\right]^T$$

$$\mathbf{A}(\mathbf{x}) = \sum_{a=1}^{n} v^a(\mathbf{x})\mathbf{p}(\mathbf{x}^a)\mathbf{p}^T(\mathbf{x}^a),$$

$$\mathbf{B}(\mathbf{x}) = \left[v^1(\mathbf{x})\mathbf{p}(\mathbf{x}^1),\, v^2(\mathbf{x})\mathbf{p}(\mathbf{x}^2), ..., v^n(\mathbf{x})\mathbf{p}(\mathbf{x}^n)\right]. \tag{22}$$

The MLS approximation is well defined only when the matrix $\mathbf{A}$ in eq. (21) is non-singular. A necessary condition to satisfy this requirement is that at least m weight functions are non-zero (i.e., $n \geq m$) for each sample point $\mathbf{x} \in \Omega$ and that the nodes in Ω_x are not arranged in a special pattern such as on a straight line.

The solution of eq. (21) for $\mathbf{a}(\mathbf{x},s)$ and a subsequent substitution into eq. (18) lead to the following relation

$$\overline{\mathbf{w}}^h(\mathbf{x},s) = \boldsymbol{\Phi}^T(\mathbf{x}) \cdot \hat{\mathbf{w}}(s) = \sum_{a=1}^{n} \phi^a(\mathbf{x})\hat{\mathbf{w}}^a(s)\,, \tag{23}$$

where

$$\boldsymbol{\Phi}^T(\mathbf{x}) = \mathbf{p}^T(\mathbf{x})\mathbf{A}^{-1}(\mathbf{x})\mathbf{B}(\mathbf{x})\,. \tag{24}$$

Similarly, one can obtain the approximation for the in-plane displacements

$$\overline{\mathbf{u}}^h(\mathbf{x},s) = \boldsymbol{\Phi}^T(\mathbf{x}) \cdot \hat{\mathbf{u}}(s) = \sum_{a=1}^{n} \phi^a(\mathbf{x})\hat{\mathbf{u}}^a(s)\,. \tag{25}$$

In eq. (23), $\phi^a(\mathbf{x})$ is usually referred to as the shape function of the MLS approximation corresponding to the nodal point $\mathbf{x}^a$. From eqs. (22) and (24), it can be seen that $\phi^a(\mathbf{x}) = 0$ when $v^a(\mathbf{x}) = 0$. In practical applications, $v^a(\mathbf{x})$ is often chosen in such a way that it is non-zero within the support domain of the nodal point $\mathbf{x}_i$. The support domain of the nodal point $\mathbf{x}^a$ is usually taken to be a circle of the radius r_i centred at $\mathbf{x}^a$ (see Fig. 1). The radius r_i is an important parameter of the MLS approximation because it determines the range of the interaction (coupling) between the degrees of freedom defined at considered nodes.

A 4^{th}-order spline-type weight function is applied in the present work

$$v^a(\mathbf{x}) = \begin{cases} 1-6\left(\frac{d^a}{r^a}\right)^2+8\left(\frac{d^a}{r^a}\right)^3-3\left(\frac{d^a}{r^a}\right)^4 & 0 \le d^a \le r^a \\ 0 & d^a \ge r^a \end{cases} \tag{26}$$

where $d^a = \|\mathbf{x}-\mathbf{x}^a\|$ and r^a is the radius of the circular support domain. The C^1-continuity of the weight function is ensured over the entire domain, therefore the continuity condition of the bending moments and the shear forces is satisfied. The size of the support r^a should be large enough to cover a sufficient number of nodes in the domain of definition to ensure the regularity of the matrix $\mathbf{A}$. The value of n is determined by the number of nodes lying in the support domain with radius r^a.

The partial derivatives of the MLS shape functions are obtained as [Atluri (2004)]

$$\phi^a_{,k} = \sum_{j=1}^{m}\left[p^j_{,k}(\mathbf{A}^{-1}\mathbf{B})^{ja} + p^j(\mathbf{A}^{-1}\mathbf{B}_{,k}+\mathbf{A}^{-1}_{,k}\mathbf{B})^{ja}\right], \tag{27}$$

wherein $\mathbf{A}^{-1}_{,k} = \left(\mathbf{A}^{-1}\right)_{,k}$ represents the derivative of the inverse of $\mathbf{A}$ with respect to x_k, which is given by

$$\mathbf{A}^{-1}_{,k} = -\mathbf{A}^{-1}\mathbf{A}_{,k}\mathbf{A}^{-1}.$$

The directional derivatives of $\overline{\mathbf{w}}(\mathbf{x},s)$ and $\overline{\mathbf{u}}(\mathbf{x},s)$ are approximated in terms of the same nodal values as the primary fields by

$$\overline{\mathbf{w}}_{,k}(\mathbf{x},s) = \sum_{a=1}^{n}\hat{\mathbf{w}}^a(s)\phi^a_{,k}(\mathbf{x}), \tag{28}$$

$$\overline{\mathbf{u}}_{,k}(\mathbf{x},s) = \sum_{a=1}^{n}\hat{\mathbf{u}}^a(s)\phi^a_{,k}(\mathbf{x}). \tag{29}$$

Substituting approximation (28) into the definition for the normal bending moments $\left[\overline{M}_1(\mathbf{x},s),\ \overline{M}_2(\mathbf{x},s)\right]^T$ and using Eq. (2), one obtains

$$\begin{aligned}\overline{\mathbf{M}}(\mathbf{x},s) &= \mathbf{N_1}\sum_{a=1}^{n}\mathbf{H}^a_1(\mathbf{x})\mathbf{w}^{*a}(s) + \mathbf{N_2}\sum_{a=1}^{n}\mathbf{H}^a_2(\mathbf{x})\mathbf{w}^{*a}(s)\\ &= \mathbf{N}_\alpha(\mathbf{x})\sum_{a=1}^{n}\mathbf{H}^a_\alpha(\mathbf{x})\mathbf{w}^{*a}(s),\end{aligned} \tag{30}$$

where the vector $\mathbf{w}^{*a}(s)$is defined as a column vector $\mathbf{w}^{*a}(s) = [\hat{w}^a_1(s),\ \hat{w}^a_2(s)]^T$, the matrices $\mathbf{N}_\alpha(\mathbf{x})$ are related to the normal vector $\mathbf{n(x)}$ on $\partial\Omega_s$ by

$$\mathbf{N}_1(\mathbf{x}) = \begin{bmatrix} n_1 & 0 & n_2 \\ 0 & n_2 & n_1 \end{bmatrix} \quad \text{and} \quad \mathbf{N}_2(\mathbf{x}) = \begin{bmatrix} n_1 & n_1 \\ n_2 & n_2 \end{bmatrix},$$

and the matrices $\mathbf{H}^a_\alpha$ are represented by the gradients of the shape functions as

$$\mathbf{H}^a_1(\mathbf{x}) = \frac{1-\nu}{2}D\begin{bmatrix} 2\phi^a_{,1} & 0 \\ 0 & 2\phi^a_{,2} \\ \phi^a_{,2} & \phi^a_{,1} \end{bmatrix},$$

$$\mathbf{H}^a_2(\mathbf{x}) = \nu D\begin{bmatrix} \phi^a_{,1} & 0 \\ 0 & \phi^a_{,2} \end{bmatrix}.$$

Similarly one can obtain the approximation for the shear forces $\left[\overline{Q}_1(\mathbf{x},s),\ \overline{Q}_2(\mathbf{x},s)\right]^T$

$$\overline{\mathbf{Q}}(\mathbf{x},s) = \frac{1-\nu}{2}D\lambda^2\sum_{a=1}^{n}\left[\phi^a(\mathbf{x})\mathbf{w}^{*a}(s) + \mathbf{F}^a(\mathbf{x})\hat{w}^a_3(s)\right], \tag{31}$$

where $\mathbf{F}^a(\mathbf{x}) = \left[\phi^a_{,1},\ \phi^a_{,2}\right]^T$, and the traction vector $\left[\overline{P}_1(\mathbf{x},s),\ \overline{P}_2(\mathbf{x},s)\right]^T$

$$\begin{aligned}\overline{\mathbf{P}}(\mathbf{x},s) &= \frac{B}{D}\mathbf{N}_\alpha(\mathbf{x})\sum_{a=1}^{n}\mathbf{H}^a_\alpha(\mathbf{x})\mathbf{u}^{*a}(s)\\ &\quad + \mathbf{G}(\mathbf{x})\sum_{a=1}^{n}\phi^a(\mathbf{x})\hat{w}^a_3(s),\end{aligned} \tag{32}$$

where the vector $\mathbf{u}^{*a}(s)$is defined as a column vector $\mathbf{u}^{*a}(s) = [\hat{u}^a_1(s),\ \hat{u}^a_2(s)]^T$, and $\mathbf{G}(\mathbf{x})$is given by

$$\mathbf{G}(\mathbf{x}) = B\begin{bmatrix} (k_{11}+\nu k_{22})n_1 + (1-\nu)k_{12}n_2 \\ (k_{22}+\nu k_{11})n_2 + (1-\nu)k_{21}n_1 \end{bmatrix}.$$

We need to approximate also

$$\begin{aligned}k_{\alpha\beta}(\mathbf{x})\overline{N}_{\alpha\beta}(\mathbf{x},s) &= \sum_{a=1}^{n}\mathbf{K}^a(\mathbf{x})^T\mathbf{u}^{*a}(s)\\ &\quad + C(\mathbf{x})\sum_{a=1}^{n}\phi^a(\mathbf{x})\hat{w}^a_3(s),\end{aligned} \tag{33}$$

where

$$\mathbf{K}^a(\mathbf{x}) = \frac{B}{2}\begin{bmatrix} 2(k_{11}+\nu k_{22})\phi^a_{,1}+(1-\nu)(k_{12}+k_{21})\phi^a_{,2} \\ \\ 2(k_{22}+\nu k_{11})\phi^a_{,2}+(1-\nu)(k_{12}+k_{21})\phi^a_{,1} \end{bmatrix}$$

$$C(\mathbf{x}) = B\left[(1-\nu)k_{\alpha\beta}(\mathbf{x})k_{\alpha\beta}(\mathbf{x})+\nu k_{\alpha\alpha}(\mathbf{x})k_{\gamma\gamma}(\mathbf{x})\right] \quad .$$

Furthermore, in view of the MLS-approximations (30) - (33) for terms occurring in the local boundary-domain integral equations (15) - (17), we obtain the following discretized local integral equations (LIEs)

$$\begin{aligned}
&\sum_{a=1}^{n}\left[\int\limits_{L^i_s+\Gamma^i_{sw}} \mathbf{N}_\alpha(\mathbf{x})\mathbf{H}^a_\alpha(\mathbf{x})d\Gamma\right. \\
&\left.-\left(\frac{1-\nu}{2}D\lambda^2+\frac{\rho h^3}{12}s^2\right)\mathbf{E}\int\limits_{\Omega^i_s}\phi^a(\mathbf{x})d\Omega\right]\mathbf{w}^{*a}(s) \\
&-\frac{1-\nu}{2}D\lambda^2\sum_{a=1}^{n}\hat{w}^a_3(s)\int\limits_{\Omega^i_s}\mathbf{F}^a(\mathbf{x})d\Omega \\
&=-\int\limits_{\Gamma^i_{sM}}\tilde{\overline{\mathbf{M}}}(\mathbf{x},s)d\Gamma-\int\limits_{\Omega^i_s}\overline{\mathbf{R}}(\mathbf{x},s)d\Omega, \qquad (34)
\end{aligned}$$

$$\begin{aligned}
&\frac{1-\nu}{2}D\lambda^2\sum_{a=1}^{n}\left[\int\limits_{\partial\Omega^i_s}\mathbf{N}(\mathbf{x})^T\phi^a(\mathbf{x})d\Omega\right]\mathbf{w}^{*a}(s) \\
&-\sum_{a=1}^{n}\left[\int\limits_{\Omega^i_s}\mathbf{K}^a(\mathbf{x})^T d\Omega\right]\mathbf{u}^{*a}(s) \\
&+\sum_{a=1}^{n}\hat{w}^a_3(s)\left(\frac{1-\nu}{2}D\lambda^2\int\limits_{\partial\Omega^i_s}\phi^a_{,\alpha}(\mathbf{x})n_\alpha(\mathbf{x})d\Omega\right. \\
&\left.-\int\limits_{\Omega^i_s}C(\mathbf{x})\phi^a(\mathbf{x})d\Omega-\rho hs^2\int\limits_{\Omega^i_s}\phi^a(\mathbf{x})d\Omega\right) \\
&=-\int\limits_{\Omega^i_s}\overline{R}_3(\mathbf{x},s)d\Omega, \qquad (35)
\end{aligned}$$

$$\begin{aligned}
&\sum_{a=1}^{n}\left[\frac{B}{D}\int\limits_{L^i_s+\Gamma^i_{su}}\mathbf{N}_\alpha(\mathbf{x})\mathbf{H}^a_\alpha(\mathbf{x})d\Gamma-\rho s^2\mathbf{E}\int\limits_{\Omega^i_s}\phi^a(\mathbf{x})d\Omega\right]\mathbf{u}^{*a}(s) \\
&+\sum_{a=1}^{n}\hat{w}^a_3(s)\int\limits_{\Omega^i_s}\mathbf{G}(\mathbf{x})\phi^a(\mathbf{x})d\Omega \\
&=-\int\limits_{\Gamma^i_{sP}}\tilde{\overline{\mathbf{P}}}(\mathbf{x},s)d\Gamma-\int\limits_{\Omega^i_s}\overline{\mathbf{R}}'(\mathbf{x},s)d\Omega, \qquad (36)
\end{aligned}$$

in which $\mathbf{E}$ is the unit 2×2 matrix and $\mathbf{N}(\mathbf{x})^T = [n_1(\mathbf{x}), n_2(\mathbf{x})]$. Recall that the LIE (34)-(36) are considered on the sub-domains adjacent to the interior nodes $\mathbf{x}^i$ as well as to the boundary nodes on Γ^i_{sM} and Γ^i_{sP}. For the source point $\mathbf{x}^i$ located on the global boundary Γ the boundary of the subdomain $\partial\Omega^i_s$ is composed of the interior and boundary portions L^i_s and Γ^i_{sM}, respectively, or alternatively of L^i_s and Γ^i_{sP}, with the portions Γ^i_{sM} and Γ^i_{sP}lying on the global boundary with prescribed bending moments or stress vector, respectively, as shown in Fig. 1. The LIEs (34) and (36) are vector equations for two components of rotations and in-plane displacements, respectively. Then, set of LIEs (34)-(36) represents 5 equations in each node for five unknown components, two rotations, deflection and two in-plane displacements.

It should be noted here that there are neither Lagrange-multipliers nor penalty parameters introduced into the local weak-forms (8) - (10) because the essential boundary conditions on Γ^i_{sw} or Γ^i_{su}can be imposed directly by using the interpolation approximation (23) and (25):

$$\sum_{a=1}^{n}\phi^a(\mathbf{x})\hat{\mathbf{w}}^a(s) = \tilde{\overline{\mathbf{w}}}(\mathbf{x}^i,s) \quad \text{for } \mathbf{x}^i\in\Gamma^i_{sw}, \qquad (37)$$

$$\sum_{a=1}^{n}\phi^a(\mathbf{x})\hat{\mathbf{u}}^a(s) = \tilde{\overline{\mathbf{u}}}(\mathbf{x}^i,s) \quad \text{for } \mathbf{x}^i\in\Gamma^i_{su}, \qquad (38)$$

where $\tilde{\overline{\mathbf{w}}}(\mathbf{x}^i,s)$ and $\tilde{\overline{\mathbf{u}}}(\mathbf{x}^i,s)$ are the Laplace transforms of the generalized displacement vector prescribed on the boundary Γ^i_{sw} and Γ^i_{su} , respectively. For a clamped plate all three vector components (rotations and deflection) and two components of in-plane displacements are vanishing at the fixed edge and only equations (37) and (38) are used at the boundary nodes in such a case. However, for a simply supported plate only the third component of the generalized displacement vector (deflection) is prescribed and the rotations are unknown. Then, equations

(34) , (36) together with eq. (37) for the third vector component are applied for a point on the global boundary. If no geometrical boundary conditions are prescribed on the part of the boundary, all tree local integral equations (34) - (36) are applied.

The time-dependent values of the transformed quantities in the previous consideration can be obtained by an inverse transform. There are many inversion methods available for the inverse Laplace-transform. As the inverse Laplace-transform is an ill-posed problem, small truncation errors can be greatly magnified in the inversion process and hence lead to poor numerical results. In the present analysis, the sophisticated Stehfest's algorithm [Stehfest (1970)] for the numerical inversion is used. If $\overline{f}(s)$ is the Laplace-transform of $f(t)$, an approximate value f_a of $f(t)$ for a specific time t is given by

$$f_a(t) = \frac{\ln 2}{t} \sum_{i=1}^{N} v_i \overline{f}\left(\frac{\ln 2}{t} i\right) \quad , \tag{39}$$

where

$$v_i = (-1)^{N/2+i} \times \sum_{k=[(i+1)/2]}^{\min(i,N/2)} \frac{k^{N/2}(2k)!}{(N/2-k)!\,k!\,(k-1)!\,(i-k)!\,(2k-i)!}. \tag{40}$$

In numerical analyses, we have considered N = 10 for single precision arithmetic. It means that for each time t it is needed to solve N boundary value problems for the corresponding Laplace-transform parameters $s = i\ln 2/t$, with $i = 1, 2, ..., N$. If M denotes the number of the time instants in which we are interested to know $f(t)$, the number of the Laplace- transform solutions $\overline{f}(s_j)$ is then $M \times N$.

4 Numerical examples

Numerical results are presented for shallow spherical shells under static and impact loads with the Heaviside-type time dependence. Simply supported and/or clamped circular and square shells are analysed. In all considered cases, the shells are subjected to a uniformly distributed load.

4.1 Circular shallow spherical shell

In this example, shallow spherical cap as shown in Figure 2 is being analysed. The geometrical parameters of the cap are as follows: thickness $h = 0.1m$, radius of the circular domain $a = 5m$, curvatures $k_{\alpha\beta} = \delta_{\alpha\beta}/R$, and we considered two analyses with respect to the radius of the cap $R = 100m$ and $1000m$. The cap is loaded with uniform pressure $q_3 = 1MPa$. The following material parameters are used in our numerical analysis: Young's modulus $E = 10^5\,\mathrm{N/m^2}$ and Poisson's ratio $\nu = 0.25$. For the purpose of error estimation and convergence studies the Sobolev-norm is calculated. The relative error of the deflection is defined as

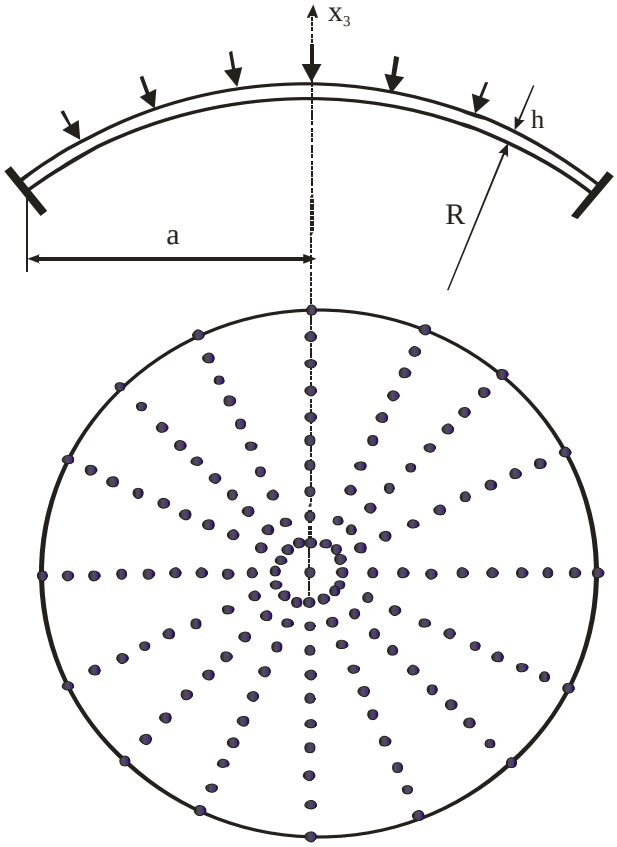

Figure 2 : Node distribution for numerical analyses of a circular shallow spherical shell

$$r = \frac{\left\| w_3^{num} - w_3^{bench} \right\|}{\left\| w_3^{bench} \right\|}, \tag{41}$$

where

$$\|w_3\| = \left(\int_\Omega w_3^2 d\Omega \right)^{1/2} .$$

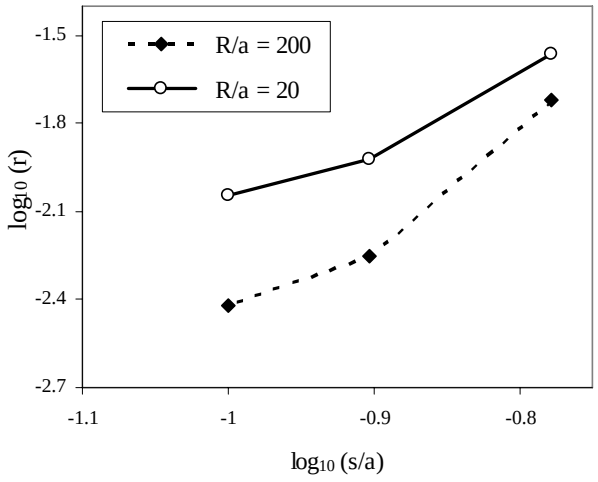

Figure 3 : Relative errors and convergence rates for the central deflection of circular shallow shells with simply supported edge

As a benchmark solution, the BEM results [Dirgantara and Aliabadi (1999)] have been used, where a fine mesh-discretization with 16 boundary elements and 30 cells is applied. To study the convergence of the method for the shell with simply supported edges, three regular node distributions with 99, 129, and 161 nodes, respectively, are used for the MLS approximation of the quantities. For a regular node distribution (see Fig. 2), the density of nodes can be characterized by the distance of two neighbouring nodes s on the radius. The relative errors and the convergence rates for deflections of two different curved caps are given in Fig. 3. For the finest node distribution with total 161 nodes the relative error for deflection is 0.39% in case of the curvature $R/a = 200$, and 0.9% for the curvature $R/a = 20$. Variation of the deflection with the radius r along the radial coordinate is given in Fig 4. The numerical results for the small curvature of shell, $R/a = 200$, are in very good agreement with those obtained by BEM and FEM. For FEM analysis we have used 120 quadrilateral shell elements. For the more curved shell, $R/a = 20$ (Fig. 4b), a good agreement of the present results is observed only with BEM. The central deflection obtained by FEM is about 9% lower than BEM and MLPG results.

Also the clamped boundary conditions were used in numerical analysis. The same geometrical and material parameters are considered here as for a simply supported

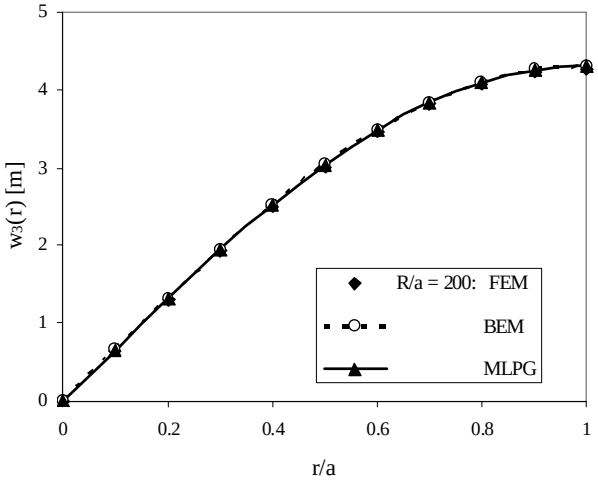

(a)

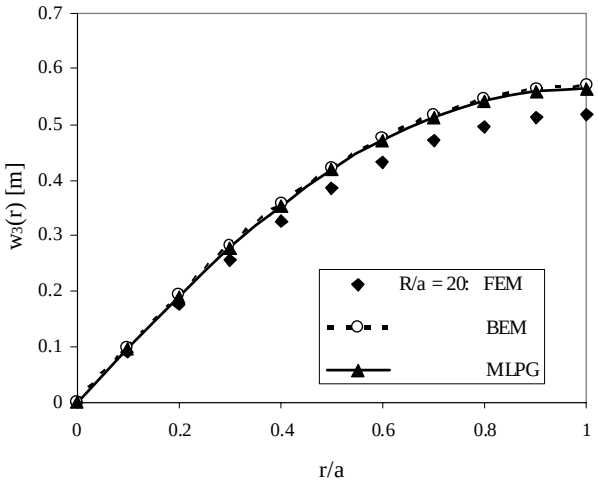

(b)

Figure 4 : Variation of deflection with radius r for simply supported shallow spherical shell: a) $R/a = 200$ b) $R/a = 20$

shell. The variation of the deflections along the radial coordinate r is given in Fig. 5. A better agreement of all 3 numerical results for both curvatures of the shell is observed in this case than in the case of simply supported shell. The same problem was also analysed by Zhang and Atluri (1986).

4.2 Square shallow spherical shell

A shallow spherical shell with square contour is analyzed here (Fig.6). The following geometrical and material parameters are assumed: side length of the

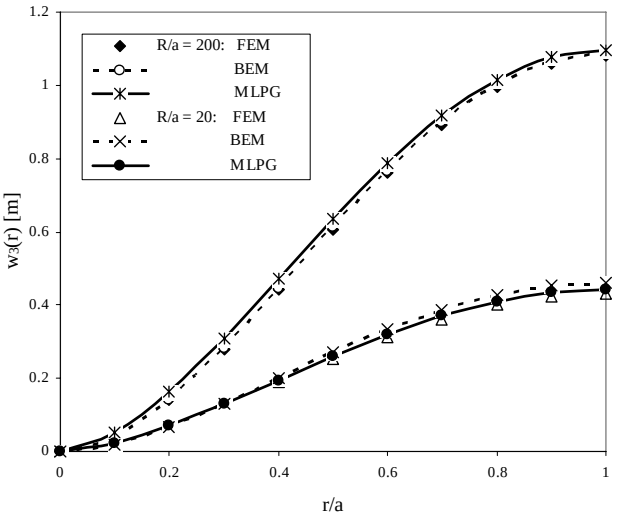

Figure 5 : Variation of the deflection along the radial coordinate for two clamped shallow spherical shells with different curvatures $R/a = 200$ and $R/a = 20$

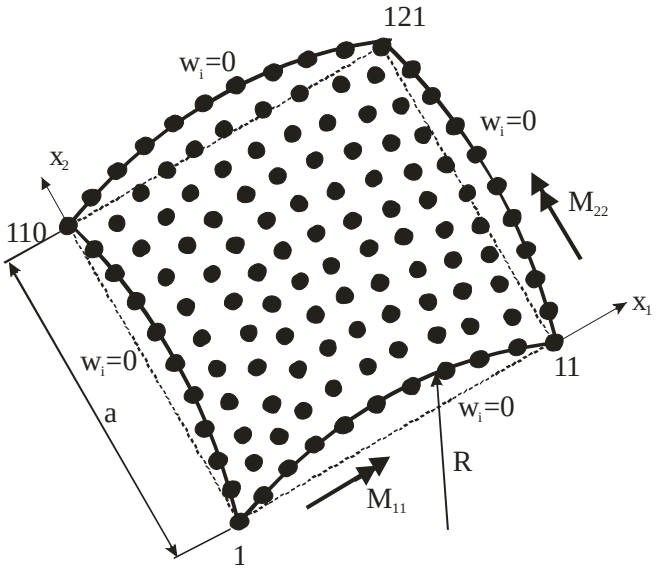

Figure 6 : Geometry and boundary conditions used for the square shallow spherical shell

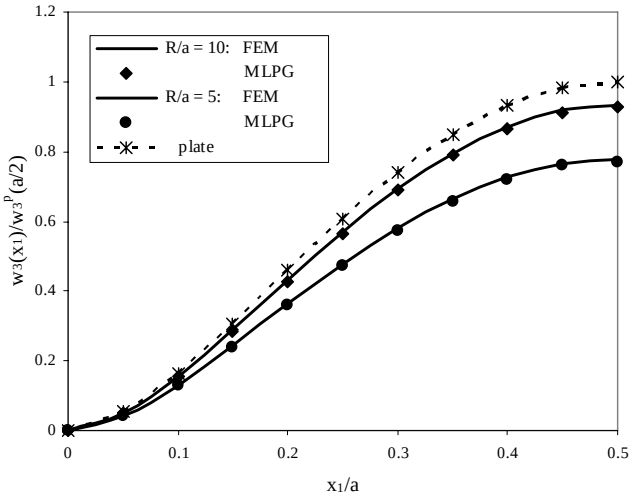

Figure 7 : Variation of the deflection along the x_1-coordinate for a clamped square shallow spherical shell

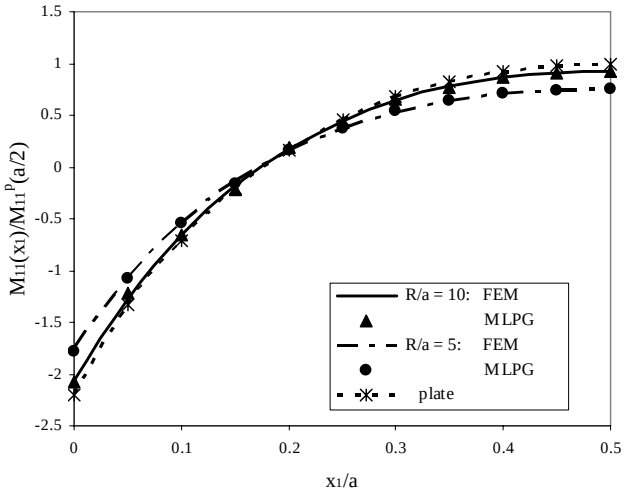

Figure 8 : Variation of the bending moment M_{11} along the x_1-coordinate for a clamped square shallow spherical shell

plate $a = 0.254$m, thickness $h = 0.0127$m, mass density $\rho = 7.166 \times 10^4\,\mathrm{N/m^3}$, modulus of elasticity $E = 0.6895 \times 10^{10}\,\mathrm{N/m^2}$, and Poisson's ratio $\nu = 0.3$. The amplitude of the uniformly distributed load q_0 is equal to $2.07 \times 10^6\,\mathrm{N/m^2}$. For numerical analyses we have used the regular node distribution with the total number of 441 nodes. In the first, a clamped shallow shell under a uniform static load is analysed. Variation of the deflection along the x_1-coordinate at $x_2 = a/2$ is presented in Fig.7 for two shells with different curvatures $R/a = 5$ and 10. Shell deflections are normalized to the central deflection of the corresponding plate ($R = \infty$) with $w_3^p(a/2) = 8.842 \cdot 10^{-3} m$. Higher reduction of the relative deflections is confirmed for the shell of higher curvature (smaller radius R). The variation of the bending moment M_{11} along the x_1-coordinate at $x_2 = a/2$ is presented in Fig.8. Again the bending moment is normalized by the plate bending moment value at the center of plate, $M_{11}^p = 3064Nm$. The absolute values of the bending moments at the shell center as well as on

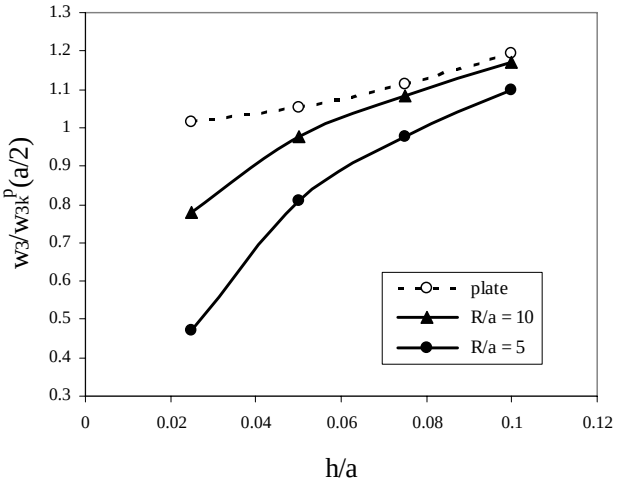

Figure 9 : Influence of the shell thickness on the central deflection of a clamped square shallow spherical shell

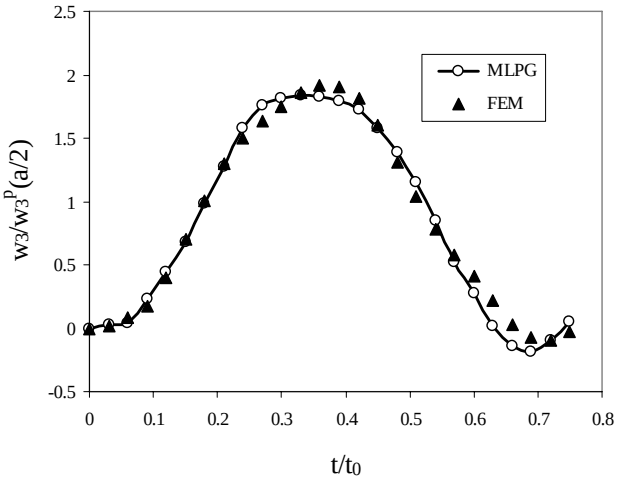

Figure 10 : Time-variation of central deflection of clamped square shallow spherical shell with curvature $R/a = 10$ and subjected to a suddenly applied uniform load

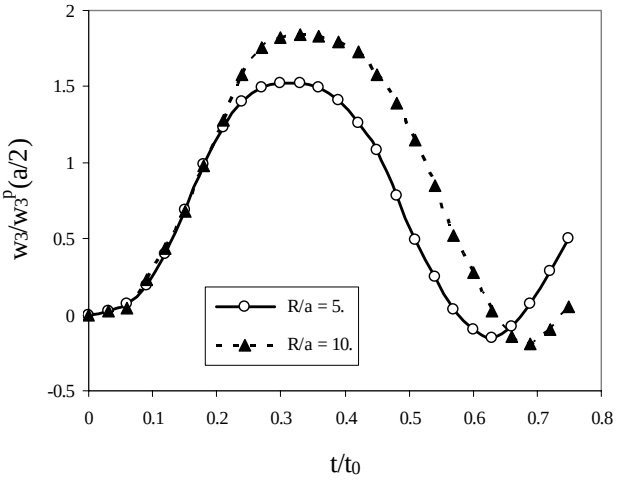

Figure 11 : Influence of the shell curvatures on the time variation of central deflection of clamped square shallow spherical shell

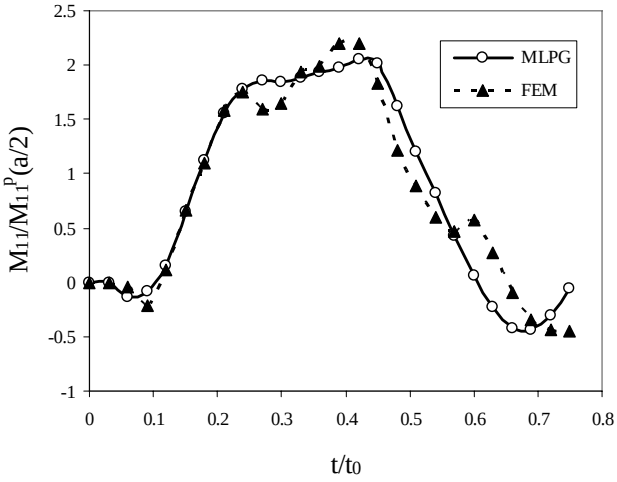

Figure 12 : Time-variation of central bending moment M_{11} of clamped square shallow spherical shell with curvature $R/a = 10$ subjected to a suddenly applied uniform load

the clamped side are slightly reduced for the shell with higher curvature. The present MLPG results are compared with those obtained by the FEM-NASTRAN computer code with using 400 quadrilateral eight-node shell elements. Good agreements for both the deflections and bending moments are achieved, which verifies the accuracy of the present meshless method. It is interesting to note the influence of the shell thickness on the deflections computed within the Reissner theory. The variation of the central deflection with shell thickness is presented in Fig. 9, where the central deflection corresponding to the Kirchhoff theory is given by $w^p_{3K}(a/2) = 0.00126\,qa^4/D$. For a flat shell (plate) the deflection is slightly increasing with plate thickness and the Reissner values are larger than Kirchhoff ones within the whole thickness interval. Recalling that only the Reissner-Mindlin theory includes the effects of the shear deformations. For a finite value of shell curvature the normalized deflec-

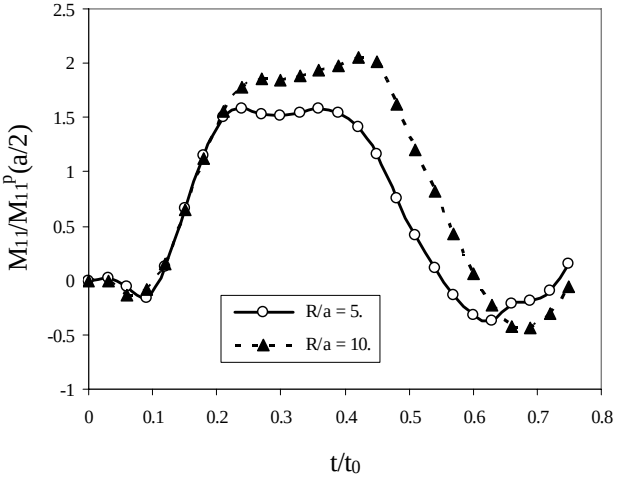

Figure 13 : Influence of the shell curvatures on the time variation of central bending moments M_{11} of clamped square shallow spherical shell

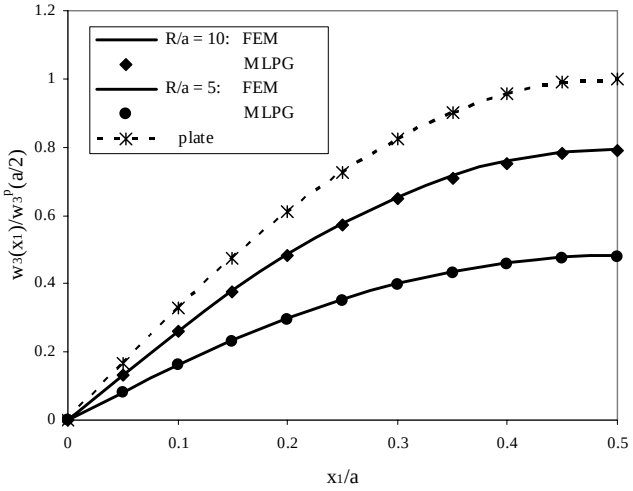

Figure 14 : Variation of deflection with x_1-coordinate for simply supported square shallow spherical shell under a static uniform load

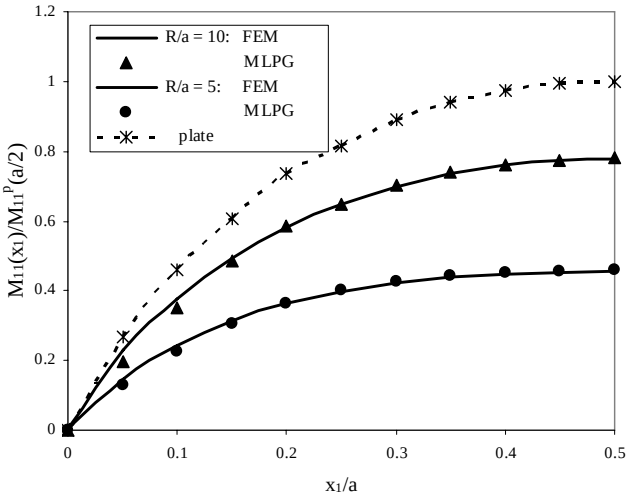

Figure 15 : Variation of bending moment M_{11} with x_1-coordinate for simply supported square shallow spherical shell under a static uniform load

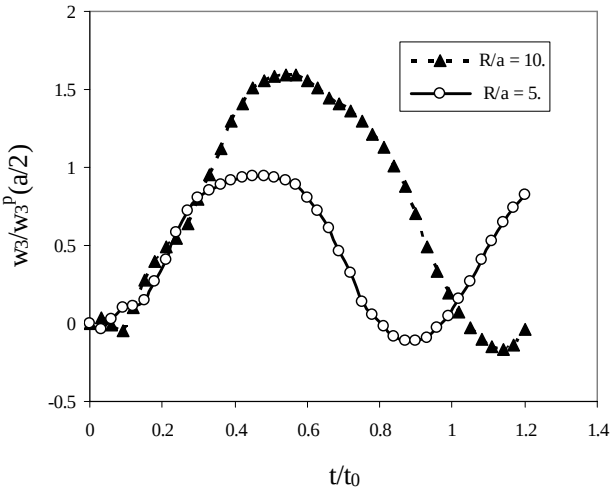

Figure 16 : Time-variation of central deflections of simply supported square shallow spherical shell under a Heaviside load

tion w_3/w_{3K}^p is growing rapidly with increasing the shell thickness mainly for small values of thickness. However, due to shell curvature its deflection cannot exceed the plate deflection.

In the next example, the uniform loading with a Heaviside time variation is applied on the clamped square shallow spherical shell considered also in the previous example. The time variation of the central deflection of the shell with the curvature $R/a = 10$ is presented in Fig. 10. The time variable is normalized by $t_0 = a^2/4\sqrt{\rho h/D} = 1.35 \cdot 10^{-2} s$. Deflections are normalized as in the static case by $w_3^p(a/2) = 8.842 \cdot 10^{-3} m$. For the FEM analysis 400 quadrilateral eight-node shell elements with 1000 time increments are used. One can observe a quite good agreement of both the MLPG and FEM results. The influence of the shell curvature on the time variation of central deflection is presented in Fig. 11. For a higher curvature of the shell, the peak value of the deflection is reached at an earlier time instant than for a more flat shell. Similar to the static case, the maximum value

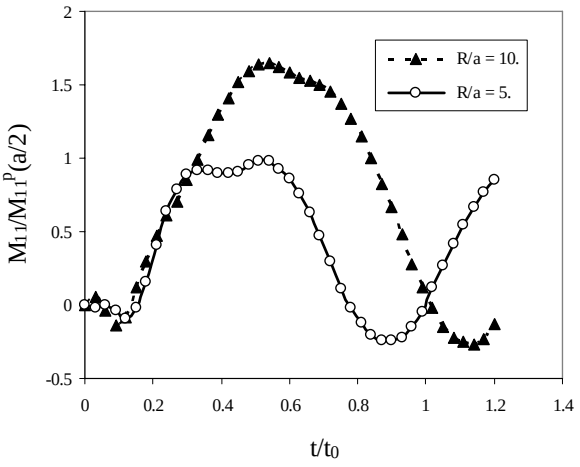

Figure 17 : Time-variation of central bending moments M_{11} of simply supported square shallow spherical shell under a Heaviside load

of the deflection is lower for more curved shell. The time-variation of the central bending moment M_{11} of the clamped square shallow spherical shell with the curvature $R/a = 10$ is presented in Fig. 12. Small discrepancies of the present MLPG and FEM results are observed here. However, the periodicity of the deflection oscillations and the maximal values are almost the same for both the results. The influence of the shell curvatures on the time variation of the central bending moments M_{11} is given in Fig. 13. The same conclusion can be made for the bending moment as for the deflection.

Now, the same plate with simply supported boundary conditions is analysed. In the first, the static uniform load is considered like in clamped shell case. The variations of the deflections along thex_1-coordinate at $x_2 = a/2$ are presented in Fig.14 for two shells with different curvatures$R/a = 5$ and 10. The deflections are normalized by the central deflection of the corresponding plate, $w_3^p(a/2) = 28.29 \cdot 10^{-3} m$. For comparison, both the deflection and bending moment are computed also by FEM. A very good agreement of the present MLPG and FEM results is observed for static case. Variation of the bending moment M_{11} along the x_1-coordinate is presented in Fig. 15. The bending moment is normalized by the plate bending moment value at the center of the plate, $M_{11}^p = 6400 Nm$. Both the deflections and bending moments are reduced with increasing the curvature of the shell.

In the last numerical example, the impact load with a Heaviside time variation is considered. The time-variation of the central deflections of two simply supported square shallow spherical shells with curvatures $R/a = 5$ and 10 are presented in Fig. 16. Similar to the case of clamped shell, one can observe higher frequency of the oscillations of deflections for the shell with higher curvature. Conversely, the amplitude of the deflection is reduced for such a shell. The same property can be observed also for the bending moment in Fig. 17.

5 Conclusions

The following conclusions can be drawn from the present study:

A meshless local Petrov-Galerkin method is applied to solving dynamic shallow shell problems described by the Reissner theory. Both the static and impact loads are considered. The influence of the shear deformation in the Reissner theory on the shell deflection is analysed too.

The Laplace-transform technique is applied to eliminate the time variable in the coupled governing differential equations of the Reissner theory. The use of the Laplace-transform in forced vibration analysis converts the dynamic problem to a set of quasi-static problems.

The analyzed domain is divided into small overlapping circular subdomains. A unit step function is used as the test function in the local weak-form. The derived local boundary-domain integral equations are nonsingular. The moving least-squares (MLS) scheme is adopted for approximating the physical quantities.

The proposed method is an alternative to existing computational methods. Its main advantage is the simplicity. The present formulation possesses the generality of the FEM. Therefore, the method seems to be promising to analyze problems, which cannot be solved effectively by the conventional BEM. Besides, the current formulation is more flexible because it allows an adaptation of the density of the nodal points. Hence, adaptive algorithms can be applied.

The present method can be easily extended to orthotropic shells. It is the subject of our further research.

Acknowledgement: The authors acknowledge the supports by the Slovak Research and Development Support Agency registered under the project number APVT-20-035404, by the Slovak Grant Agency under the

project number VEGA – 2303823.

References

Antes, H. (1981): On boundary integral equation formulation for elastic shallow shell bending problems. In *Boundary Element Methods* (Brebbia C.A., ed.), Springer, Berlin, 224-238.

Atluri, S. N.; Shen, S. (2002): *The Meshless Local Petrov-Galerkin (MLPG) Method*, Tech Science Press.

Atluri, S. N. (2004): *The Meshless Method , (MLPG) For Domain & BIE Discretizations*, Tech Science Press.

Atluri, S.N.; Sladek, J.; Sladek, V.; Zhu, T. (2000): The local boundary integral equation (LBIE) and its meshless implementation for linear elasticity. *Comput. Mech*., 25: 180-198.

Atluri, S.N.; Han, Z.D.; Shen, S. (2003): Meshless local Petrov-Galerkin (MLPG) approaches for solving the weakly-singular traction & displacement boundary integral equations. *CMES: Computer Modeling in Engineering & Sciences*, 4: 507-516.

Belytschko, T.; Krogauz, Y.; Organ, D.; Fleming, M.; Krysl, P. (1996): Meshless methods; an overview and recent developments. *Comp. Meth. Appl. Mech. Engn.*, 139: 3-47.

Beskos D.E. (1991) Static and dynamic analysis of shells, In *Boundary Element Analysis of Plates and Shells* (Beskos DE ed.). Springer-Verlag: Berlin, 1991, 93-140.

Dirgantara, T.; Aliabadi, M.H. (1999): A new boundary element formulation for shear deformable shells analysis, *International Journal for Numerical Methods in Engineering*, 45: 1257-1275.

Han, Z.D.; Atluri, S.N. (2004a): Meshless local Petrov-Galerkin (MLPG) approaches for solving 3D problems in elasto-statics. *CMES: Computer Modeling in Engineering & Sciences*, 6: 169-188.

Han, Z.D.; Atluri, S.N. (2004b): A meshless local Petrov-Galerkin (MLPG) approach for 3-dimensional elasto-dynamics. *CMC: Computers, Materials & Continua*, 1: 129-140.

Krysl, P.; Belytschko, T. (1985): Analysis of thin plates by the element-free Galerkin method, *Computational Mechanics*, 16: 1-10.

Krysl, P.; Belytschko, T. (1996): Analysis of thin shells by the element-free Galerkin method, *Int. J. Solids and Structures*, 33: 3057-3080.

Lancaster, P.; Salkauskas, T. (1981): Surfaces generated by moving least square methods, *Math. Comput.*, 37: 141-158.

Lin, J.; Long, S. (1996): Geometrically nonlinear analysis of the shallow shell by the displacement-based boundary element formulation. *Engn. Analysis with Boundary Elements*, 18: 63-70.

Long, S.Y.; Atluri, S.N. (2002): A meshless local Petrov Galerkin method for solving the bending problem of a thin plate. *CMES: Computer Modeling in Engineering & Sciences*, 3: 11-51.

Lu, P.; Huang, M. (1992): Boundary element analysis of shallow shells involving shear deformation. *Int. J. Solids and Structures*, 29: 1273-1282.

Mikhailov, S.E. (2002): Localized boundary-domain integral formulations for problems with variable coefficients. *Engn. Analysis with Boundary Elements*, 26: 681-690.

Nayroles, B.; Touzot, G.; Villon, P. (1992): Generalizing the finite element method. *Computational Mechanics*, 10: 307-318.

Newton, D.A.; Tottenham, H. (1968): Boundary value problems in thin shallow shells of arbitrary plan form. *Journal of Engineering Mathematics*, 2: 211-223.

Noguchi, H.; Kawashima, T.; Miyamura, T. (2000): Element free analyses of shell and spatial structures, *International Journal for Numerical Methods in Engineering*, 47: 1215-1240.

Providakis, C.P.; Beskos, D. (1991): Free and forced vibration of shallow shells by boundary and interior elements, *Computational Methods in Applied Mechanical Engineering*, 92: 55-74.

Reissner, E. (1946): Stresses and small displacements analysis of shallow shells-II, *Journal Math. Physics*, 25: 279-300.

Sellountos, E.J.; Polyzos, D. (2003): A MLPG (LBIE) method for solving frequency domain elastic problems, *CMES: Computer Modeling in Engineering & Sciences*, 4: 619-636.

Sellountos, E.J.; Vavourakis, V.; Polyzos, D. (2005): A new singular/hypersingular MLPG (LBIE) method for 2D elastostatics, *CMES: Computer Modeling in Engineering & Sciences*, 7: 35-48.

Sladek, J.; Sladek, V.; Mang, H.A. (2002): Mesh-

less formulations for simply supported and clamped plate problems. *Int. J. Num. Meth. Engn*., 55: 359-375.

Sladek, J.; Sladek, V.; Mang, H.A. (2003): Meshless LBIE formulations for simply supported and clamped plates under dynamic load. *Computers and Structures*, 81: 1643-1651.

Sladek, J.; Sladek, V.; Krivacek, J.; Wen, P.; Zhang, Ch. (2005): Meshless Local Petrov-Galerkin (MLPG) method for Reissner-Mindlin plates under dynamic load. *Computers and Structures*, submitted for publication.

Soric, J.; Li, Q.; Atluri, S.N. (2004): Meshless local Petrov-Galerkin (MLPG) formulation for analysis of thick plates. *CMES: Computer Modeling in Engineering & Sciences*, 6: 349-357.

Stehfest, H. (1970): Algorithm 368: numerical inversion of Laplace transform. *Comm. Assoc. Comput. Mach*., 13: 47-49.

Tosaka, H.; Miyake, S. (1983): A boundary integral equation formulation for elastic shallow shell bending problems. In *Boundary Element Methods* (Brebbia C.A., Futagami T. and Tanaka M. eds.), Springer, Berlin, 527-538.

Tottenham, H. (1979): The boundary element method for plates and shells. In *Developments in Boundary Element Methods* (Banerjee P.K. and Butterfield R., eds.), Applied Science, London, 173-205.

Wang, J.; Schweizerhof, K. (1996a): Boundary integral equation formulation for moderately thick laminated orthotropic shallow shells. *Computers and Structures*, 58: 277-287.

Wang, J.; Schweizerhof, K. (1996b): Study on free vibration of moderately thick orthotropic laminated shallow shells by boundary-domain elements, *Applied Mathematical Modelling*, 20: 579-584.

Wang, J.; Schweizerhof, K. (1996c): Boundary-domain element method for free vibration of moderately thick laminated orthotropic shallow shells, *Int. J. Solids and Structures*, 33: 11-18.

Zhang, J.D.; Atluri, S.N. (1986): A boundary/interior element method for quasi static and transient response analysis of shallow shells, *Computers and Structures*, 24: 213-223.